 MCB, vol.5, no.1, pp.27-35, 2008

Effects of Biglycan Deficiency on Myocardial Infarct Structure and Mechanics

Patrick H. Campbell[*,†], Darlene L. Hunt[*,†], Ying Jones[‡], Fred Harwood[§], David Amiel[§], Jeffrey H. Omens[†,¶] and Andrew D. McCulloch[†,‖]

Abstract: Biglycan, a small leucine-rich proteoglycan, has been shown to interact with extracellular matrix (ECM) collagen and may influence fibrillogenesis. We hypothesized that biglycan contributes to post-myocardial infarction (MI) scar development and that the absence of biglycan would result in altered scar structure and mechanics. Anterior MI was induced in biglycan hemizygous null and wild-type mice by permanent ligation of the left coronary artery. The initial extent of ischemic injury was similar in the two groups, as was the infarct size after 30 days, although there was some tendency toward reduced expansion in the biglycan-null. Electron microscopy revealed that collagen fibrils had a smaller average diameter and a narrower range in the biglycan-null scar, as well as appearing more densely packed. *In vivo* strain analysis showed that biglycan-null scars were stiffer than the wild-type. Remote LV collagen concentration tended to be reduced in biglycan-null hearts, but the difference was not statistically significant. Null-expression of biglycan may alter collagen fibril ultrastructure, and thereby influence scar mechanics and remodeling.

[*] These authors contributed equally to this work
[†] Department of Bioengineering, University of California, San Diego, La Jolla, CA 92093-0412
[‡] National Center for Microscopy and Imaging Research, University of California, San Diego, La Jolla, CA 92093-0608
[§] Department of Orthopedic Surgery, University of California, San Diego, La Jolla, CA 92093-0630
[¶] Department of Medicine, University of California, San Diego, La Jolla, CA 92093-0613-J
[‖] Corresponding author. Room 231 Powell-Focht Bioengineering Hall 9500 Gilman Drive La Jolla, CA 92093-0412 Email: amcculloch@ucsd.edu Telephone: (858) 534-2547 Fax: (858) 332-1706

1 Introduction

Under normal and pathological conditions, the structure and mechanics of the mammalian heart depend critically on the extracellular matrix (ECM). Collagen, a major component of the ECM, is organized in an intricate three-dimensional network surrounding and connecting the muscle fibers. This network facilitates the transmission of forces between fibers, and across the ventricle walls during the cardiac cycle (1, 2). In addition to its role as a force transmitter, the collagen ECM supplies the structural stability and elasticity necessary for proper pump function.

The death of myocytes during myocardial infarction (MI) induces major structural alterations collectively known as ventricular remodeling. During the acute phase after injury, necrotic tissue and its ECM are resorbed while a fibroproliferative response produces a scar rich in Type I collagen to preserve the tensile strength of the ventricle wall (3). The extent of remodeling in the ischemic region depends on the balance between these two processes. Imperfect coordination can result in thinning and elongation of the infarct region before extensive collagen deposition has occurred (3). The stiffness of the mature scar depends on collagen type, crosslinking, arrangement, and size and number of fibers (4, 5). Because it is thin and has a high local radius of curvature, the stresses observed in the scar are considerably greater than those in the unaffected region of the ventricle (4). Interestingly, in passively inflated hearts the scar was found to be anisotropic, resisting circumferential deformation more so than longitudinal or radial. Most large collagen fibers were aligned with the circumferential axis, suggesting that increased stiffness in the circumferential direction may help maintain proper ventricular mechanics (4). Thus scar structure is organized to accommodate the stresses imposed during the cardiac cycle.

There is substantial evidence that the regulation of fiber assembly and organization of fibers in infarct scar tissue, as well as other collagenous tissues, depend in part on a group of ECM macromolecules known as proteoglycans (6-9). One such macromolecule is the small leucine-rich proteoglycan (SLRP) biglycan. Biglycan is a widely expressed protein localized to the interstitium and cell surface (10). Depending on the tissue type, the biglycan core has one or two chondroitin sulfate or dermatan sulfate groups at the amino terminus (11).

Little is known about biglycan's function and its role in collagen fibrillogenesis, especially in the heart. However, biglycan binds collagen type I and TGF-β1, an important factor in driving fibrillogenesis (6, 12). The physiological or pathophysiological roles of biglycan in the heart are largely unknown, though some evidence suggests a possible function in post-MI healing. Biglycan mRNA has been shown to increase in the rat heart 2 days post-MI, with a 13-fold peak by day 14, and to co-localize with collagen type I mRNA (13).

Our lab has previously studied the role of another SLRP, decorin, in post-MI healing. Infarct scars of transgenic mice lacking decorin were structurally dysregulated, and collagen fibrils had nonuniform diameter. This may have compromised the scar's ability to resist stress, and resulted in the observed infarct expansion. Increased left ventricular dilation also led to greater hypertrophy of the remote, uninjured region (9). Since decorin has a similar structure to biglycan, even competing for binding sites on type I collagen (14), we hypothesized that similar structural dysregulation would occur in biglycan-null mice after experimental MI, and that the infarct scar mechanical properties would also be affected. In the present study, we induced MI in biglycan hemizygous-null mice and found altered collagen fibril structure in infarct scar tissue, and changes in scar mechanics compared with wild-type controls. There was evidence that lack of biglycan actually allows a denser scar with smaller, more uniform collagen fibrils that are more resistant to expansion.

2 Methods

2.1 Animals

All animal studies and husbandry were conducted under approved University of California, San Diego Animal Subjects Protocols in AAALAC-approved facilities. Breeding pairs of female homozygous biglycan-deficient ($Bgn^{-/-}$, strain name: C3.129S4(B6)-$Bgn^{tm1Mfy/Tac}$) and male hemizygous biglycan-deficient ($Bgn^{-/0}$) mice were obtained from the Mutant Mouse Regional Resource Centers through Taconic Farms, Inc., and bred at our breeding facility. Since the biglycan gene is located on the X chromosome, male biglycan-null mice are referred to as hemizygous. Male 12-18 week-old $Bgn^{-/0}$ mice were used for this study. Male age-matched C3H mice ($Bgn^{+/0}$), also obtained from Taconic, were used as controls. The C3H strain is the background of the biglycan-null, and the recommended control.

2.2 Coronary artery ligation

MI surgery was performed using a procedure similar to that described by Weis et al. (9). Mice were anesthetized with the inhalant anesthetic isoflurane at 5.0% in 95% oxygen, and maintained at 2.0% delivered to the spontaneously breathing animal through a nose cone. The trachea was surgically exposed, the tongue was retracted, and intubation was performed with a 20-gauge angiocatheter. The animal was placed on a rodent ventilator (Harvard Apparatus, Model 687), and ventilated with 2% isoflurane in 95% oxygen at a flow rate of 1 L/min and a stroke volume of 0.5 ml at 85 breaths/min. A 1.5 cm vertical left parasternal skin incision exposed the underlying pectoralis muscles, which were then retracted. The heart was exposed by entering the chest cavity through the third intercostal space and retracting adjacent ribs. The left coronary artery was ligated with 7-0 silk suture approximately 2 mm below the edge of the left atrial appendage. Ischemia was verified visually by the appearance of paleness on the surface of the left ventricle distal to the ligation. The lungs were overinflated, and the chest cavity was closed by suturing the adjacent ribs together with 6-0 prolene. The chest and neck skin incisions were then closed with prolene suture. Animals received 0.1 mg/kg buprenorphine intraoperatively for analgesia. After removal from the ventilator, animals awakened on a water-circulating heating pad (K Module, American Pharmaseal) and were placed in a clean, heated cage to recover. Surgery was performed with the aid of a stereomicroscope (Leica Microsystems MZ6).

2.3 Initial infarct size

A subset of animals (7 $Bgn^{+/0}$ and 9 $Bgn^{-/0}$) was studied one day after MI to determine the initial infarct size. Animals were anesthetized with isoflurane, the thoracic cavity was opened, and the hearts were arrested with an ice-cold, hyperkalemic Krebs-Henseleit buffer containing 2,3,5-Butanedione monoxime to delay the onset of contracture. The atria and right ventricle were removed, and the left ventricle (LV) was wrapped in plastic wrap, then placed in a -20° C freezer for 1 hour. The LV was then placed in a cutting fixture with slits spaced 1 mm apart, and sliced into 1-2 mm short axis sections. The slices were stained with triphenyl tetrazolium chloride (TTC), then squeezed between two Plexiglas plates with 1mm spacers. This apparatus was placed in a shallow tray of water and photographed with a digital camera (Nikon Coolpix 4500) mounted on a Leica MZ6 stereomicroscope (15, 16). Healthy tissue stains brick red, while unstained tissue marks the infarct area. Using ImageJ (NIH), total tissue area and infarct area were measured for both sides of each LV section and averaged. Infarct size was expressed as a percentage of infarct volume to total LV tissue volume.

2.4 Histology and light microscopy

A second group of 7 $Bgn^{+/0}$ and 8 $Bgn^{-/0}$ mice was studied 30 days after MI for measurement of infarct size. Animals were anesthetized with isoflurane, and the thoracic cavity was opened to expose the heart. Hearts were removed and arrested with the same Krebs-Henseleit buffer, then rinsed and prepared for paraffin embedding. Short axis sections 10 μm thick were taken from apex to base and stained using picrosirius red as previously described (17). A light microscope (Olympus BH-2) with a 2X objective was used in conjunction with a Spot-RT camera to obtain digital images. Infarct size was determined using a technique modified from Pfeffer (3). Image J measurements of eight to ten equally spaced sections were used to determine the infarct size, expressed as a percentage of infarct area to total LV tissue area.

2.5 Transmission electron microscopy

Infarct scar tissue from 2 animals of each genotype was isolated from the rest of the heart 30 days post-MI. The tissue was prepared as previously described (9), and imaged with Jeol-100CX microscopy to obtain cross-sectional and longitudinal views of collagen fibrils at 20,000 and 50,000X magnification. Cross-sectional diameter measurements were made with ImageJ.

2.6 Biochemistry

30 days post-MI, the remote LV was removed from 6 $Bgn^{+/0}$ and 4 $Bgn^{-/0}$ hearts. Collagen concentration, as measured by hydroxyproline content, was determined using the method of Woessner (18). Pyridinoline content was quantified to measure nonreducible crosslinks, using a method modified (19) from Eyre et al. (20).

2.7 Pressure and strain measurements

Four animals of each genotype were anesthetized and intubated as described above, and the right carotid artery was isolated. A 1.4 french Mikro-Tip conductance catheter (SPR-839, Millar instruments) was advanced down the right carotid artery to the aorta and then the LV. Continuous LV pressure was recorded at steady-state conditions, with the animal's body temperature closely monitored and maintained at 37°C with a water-circulating heating pad (K Module, American Pharmaseal). The chest was then opened to expose the heart. Titanium dioxide markers were placed on the infarct scar and videotaped using a CCD camera (COHU Inc.). Temporal resolution was increased to 60 Hz by splitting the videotape frames into fields with Scion Image (Version Beta 4.0.2). To stabilize the heart for videotaping, cotton was used as an added support and the ventilator was briefly turned off. Three marks on the infarct scar were used to determine two-dimensional epicardial area strain throughout the cardiac cycle, defined as the product of the two principal stretch ratios. The field with minimum distance between the points was used as a reference. Frame markers recorded along with the LV pressure allowed the identification of a pressure for each recorded frame (21).

2.8 Statistics

All data were analyzed with one- or two-way ANOVA or Student's t tests, with Welch's correction if necessary, at a significance level of 0.05. Data are presented as mean ± SEM.

3 Results

3.1 Infarct size

As assessed by TTC staining, there was no significant difference in the initial infarct size distribution one day post-MI between genotypes ($Bgn^{+/0}$ 32.2 ± 4.7%, n=7 vs. $Bgn^{-/0}$ 35.1 ± 5.2%, n=9; P=0.6, Figure 1). Infarct sizes were also not significantly different after 30 days, as determined by histological analysis ($Bgn^{+/0}$ 43.1 ± 1.9%, n=7 vs. $Bgn^{-/0}$40.2 ± 2.8%, n=8; P=0.4, Figure 2). The change in infarct size from 1 to 30 days post-MI was twice as great in $Bgn^{+/0}$ hearts compared to $Bgn^{-/0}$ hearts, but since it was not possible to study the same animals at the two time points, this difference was not significant (P∼0.5).

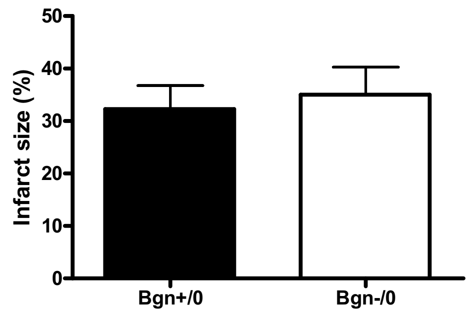

Figure 1: One day following MI, infarct size as measured by TTC staining was not significantly different between genotypes ($Bgn^{+/0}$: n=7, $Bgn^{-/0}$: n=9, P=0.6).

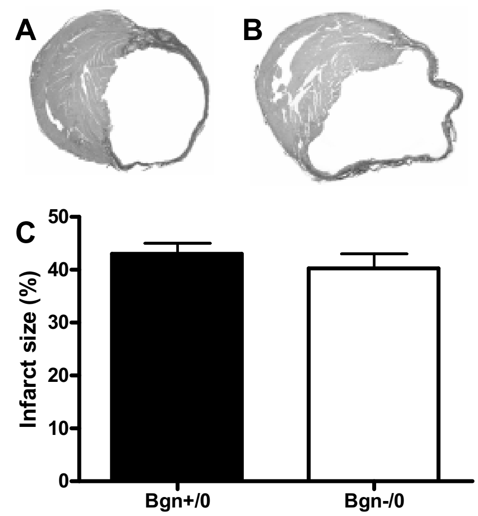

Figure 2: 30 days after MI, scar size was similar between genotypes. Representative micrographs of $Bgn^{+/0}$ (A) and $Bgn^{-/0}$ (B) hearts stained with picrosirius red. Infarct size measured from histological sections (C) was not significantly different ($Bgn^{+/0}$: n=7, $Bgn^{-/0}$: n=8, P=0.4).

3.2 Infarct scar ultrastructure

The ultrastructure of $Bgn^{+/0}$ and $Bgn^{-/0}$ infarct scars was investigated using electron microscopy. A longitudinal view of collagen fibrils from each genotype is shown in Figure 3. No differences were observed in the longitudinal structure of the individual fibrils and the arrangement of fibrils forming the scar tissue. However, a cross-sectional view revealed that collagen fibril diameter was smaller in $Bgn^{-/0}$ scars (Figure 4B) than in $Bgn^{+/0}$ scars (Figure 4A). Measurement of a random sample of 100 fibrils from 2 animals of each genotype showed that both their diameter and cross-sectional area were significantly smaller in $Bgn^{-/0}$ than $Bgn^{+/0}$ scars (diameter: 37.7 ± 0.6 nm vs. 46.9 ± 0.8 nm, P<0.0001; area: 1138 ± 33 nm^2 vs. 1773 ± 55 nm^2, P<0.0001; Figure 4C, D). Interestingly, the variance in fibril diameter and cross-sectional area was significantly smaller in $Bgn^{-/0}$ scars (P<0.005). Histograms showed that the two highest frequency bins (35 and 40 nm) comprised 68%

of $Bgn^{-/0}$ fibril diameters (Figure 4F), while the two $Bgn^{+/0}$ high frequency bins (45 and 50 nm) included only 48% of fibrils (Figure 4E). From the representative images in Figure 4A and B, it appears that the fibrils are more closely packed in $Bgn^{-/0}$ than $Bgn^{+/0}$ scars, though this was not quantified.

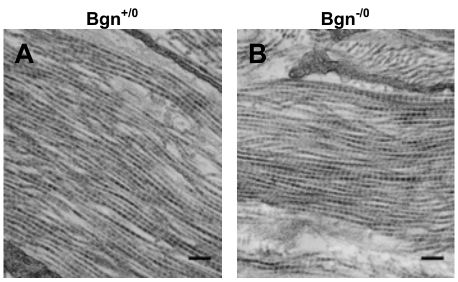

Figure 3: There were no apparent differences between genotypes in longitudinal collagen fibril ultrastructure of the scar 30 days post-MI. Representative electron micrographs (20,000X) of $Bgn^{+/0}$ (A) and $Bgn^{-/0}$ (B); bar=200 nm.

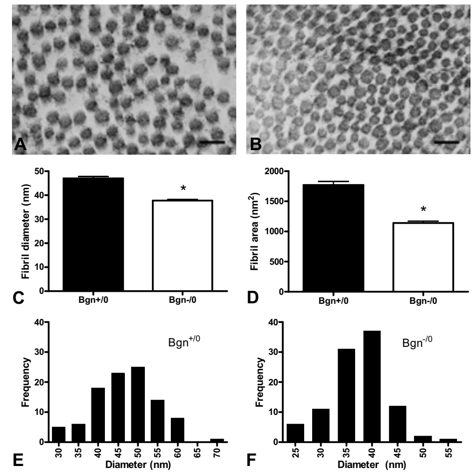

Figure 4: Collagen fibril ultrastructure is altered in $Bgn^{-/0}$ scars. Fibril diameter (C) and area (D) were significantly smaller in $Bgn^{+/0}$ scars compared to $Bgn^{-/0}$(n=100, P<0.0001 diameter and area). Representative electron micrographs (50,000X) of $Bgn^{+/0}$ (A) and $Bgn^{-/0}$ (B) scars; bar=100 nm. Fibrils appear to be more closely packed in $Bgn^{-/0}$ scars. The distribution of fibril diameters was different between genotypes (E, F). The variance in diameter was significantly smaller in $Bgn^{-/0}$ scars (F, P<0.005).

3.3 LV collagen concentration

Collagen concentration was measured in both the infarct and non-infarct region of the LV in both genotypes (Figure 5), and crosslinking was quantified in the infarct region. The concentration is expressed as a percentage of total non-infarcted LV dry weight. Collagen concentration was not significantly different in the infarct region of $Bgn^{+/0}$ and $Bgn^{-/0}$ hearts (30.02 ± 1.95%, n=6 vs. 32.95 ± 3.00%, n=7, P=0.4; Figure 5A). There was a trend toward greater collagen concentration in the remote region of $Bgn^{+/0}$ hearts compared to the $Bgn^{-/0}$ hearts (1.80 ± 0.12%, n=6 vs. 1.47 ± 0.07%, n=4, P=0.07; Figure 5B). Collagen crosslinking, as determined by pyridinoline content, was not significantly different between genotypes (0.43 ± 0.15%, n=3 vs. 0.34 ± 0.7%, n=7, P=0.6; data not shown).

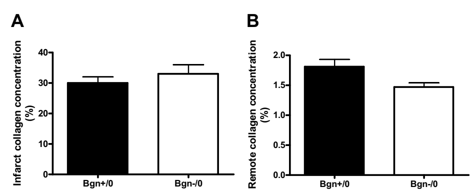

Figure 5: Collagen concentration, measured by hydroxyproline content, in the infarct region 30 days post-MI was not significantly different between genotypes (A, $Bgn^{+/0}$ n=6, $Bgn^{-/0}$ n=7, P=0.4). $Bgn^{-/0}$ left ventricles tended to have less collagen deposition in the remote region (B), but the difference was not statistically significant ($Bgn^{+/0}$: n=6, $Bgn^{-/0}$: n=4, P=0.07).

3.4 Strain analysis

In vivo strain analysis was performed directly on the infarct scar 30 days post-MI in $Bgn^{+/0}$ and $Bgn^{-/0}$ mice. Averaged area strain for 4 animals of each genotype over approximately 4 cardiac cycles is shown in Figure 6. ANOVA showed there was a significant difference between the curves; strain was significantly smaller in $Bgn^{-/0}$ than in $Bgn^{+/0}$ scars (P=0.005). Consistent with the collagen fibril diameter results presented above, the variability in strain was smaller in $Bgn^{-/0}$ scars than in $Bgn^{+/0}$ scars. Simultaneous conductance catheter pressure measurements were averaged in a similar manner and plotted against strain; Figure 7 depicts the pressure-strain curve for each genotype. Two-way ANOVA showed that $Bgn^{-/0}$ scars were significantly stiffer (P=0.01).

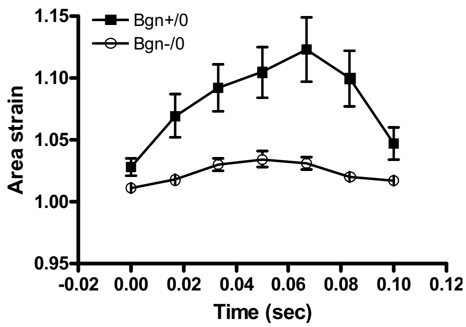

Figure 6: Average *in vivo* area strain over time, measured by surface markers placed directly on the scar. 4 beats from each of 4 $Bgn^{+/0}$ and 4 $Bgn^{-/0}$ hearts were averaged. There was a significant difference between the curves by ANOVA; strain was smaller in $Bgn^{-/0}$ scars (P=0.005). The variability in strain was also smaller in $Bgn^{-/0}$ scars.

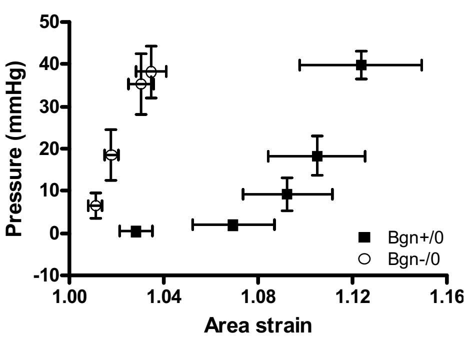

Figure 7: Average *in vivo* pressure-strain curves, measured by a conductance catheter and surface markers. 4 beats from each of 4 $Bgn^{+/0}$ and 4 $Bgn^{-/0}$ hearts were averaged. $Bgn^{-/0}$ scars were significantly stiffer by ANOVA (P=0.01).

4 Discussion

This study investigated the role of the SLRP biglycan in post-myocardial infarction healing and remodeling. Collagen fibril diameter and cross-sectional area were significantly smaller in $Bgn^{-/0}$ infarct scars 30 days post-MI than in $Bgn^{+/0}$ scars. Fibrils were also more closely packed, which may have led to the significantly increased stiffness and reduced variability of $Bgn^{-/0}$ scars observed during *in-vivo* strain analysis. These scars expanded half as much as their $Bgn^{+/0}$ counterparts. However, owing to the inherent variability of infarct size in coronary ligation studies, and since we did not have a means for longitudinal measurement of infarct size *in vivo* throughout the study period, the sample size was not large enough for this difference in post-infarct remodeling to achieve statistical significance. A trend toward reduced collagen concentration in the remote LV further supported this reduction in remodeling severity. Here we show for the first time that lack of biglycan induces ultrastructural changes in the mouse heart, and that these may lead to a stiffer scar that resists expansion more effectively than the wild-type, thereby reducing the severity of remodeling in the chronic phase of MI.

Little research exists on the collagen ultrastructure of the biglycan-null mouse, but there are some similarities between the present study and previous reports (22, 23). Smaller collagen fibril diameters were observed in the proximal predentin of $Bgn^{-/0}$ mice compared to $Bgn^{+/0}$, while other regions had larger diameters (22). Ameye and colleagues (23) reported that patellar tendons from biglycan/fibromodulin double-knockout mice had a significantly different range and distribution of collagen fibrils than wild-type, and that double-knockout fibrils were smaller. In the endometrium of the uterus, the loss of thin collagen fibers and an increase in thick fibers was correlated with the appearance of biglycan and the loss of two other SLRPs, decorin and lumican (14). Finally, the reported range of collagen fibril diameters in the normal mammalian heart is 30-70 nm (24), consistent with the $Bgn^{+/0}$ infarct scars in the present study.

Our laboratory has examined another SLRP, decorin, and its role in post-MI healing. Decorin-null infarct scar ultrastructure was clearly dysregulated compared to wild-type controls, and we hypothesized that this altered the scar mechanical properties, thereby causing severe infarct thinning and expansion (9). Decorin-null collagen fibrils had a larger range of diameters, and were more loosely packed than their wild-type counterparts. The reason for the disparity between decorin- and biglycan-null scars may lie in the two SLRPs' collagen-binding properties. Decorin and biglycan have been shown to compete for binding sites on type I collagen (6). Furthermore, the association of decorin with type I collagen produces thinner fibrils, possibly because it inhibits lateral aggregation during their formation (25). Together, these data suggest that the removal of biglycan frees additional binding sites for decorin, which then prevents the enlargement of fibril diameter to the extent biglycan would allow.

Collagen type I is the major structural component of the mature infarct scar, and the scar mechanical properties depend on a variety of characteristics of the collagen molecule, fibril organization, and the arrangement of scar fibers (4, 26). It could be expected that tissue with predominantly smaller diameter collagen fibrils may be less stiff, and this has been demonstrated in biglycan/fibromodulin double-knockout patellar tendons compared to the wild-type (23). However, the data presented in the present study indicate $Bgn^{-/0}$ scars were actually stiffer than $Bgn^{+/0}$. A greater density of fibrils may have compensated for this. The number of fibrils per unit area was not quantified, but inspection of representative cross-sectional EM images in Figures 3A and B shows that greater fibril density is likely in $Bgn^{-/0}$ scars.

Collagen fibril organization could be another important factor in the stiffness and integrity of $Bgn^{-/0}$ scars. Fibrils of decorin-null scars were loosely packed and disorganized, and significant infarct expansion was observed (9). Similar disorganization did not occur in $Bgn^{-/0}$ scars. Proper fibril orientation may be required for the scar to withstand the deformations imposed by the cardiac cycle. Holmes and colleagues found that fibril orientation is an important factor in the strain distribution of infarct scars—the largest fibrils were found in the direction of smallest strain (4). Since there was no apparent disruption of fibril organization in $Bgn^{-/0}$ scars, their integrity was likely maintained.

In contrast to the decorin-null, $Bgn^{-/0}$ infarcts did not expand compared with the wild-type, and may have even expanded less. This could be related to the stiffness of the scar. Models have shown that stiffer scars can restrict systolic stretching (27), while compliant scars have more negative effects on systolic function (28). These data suggest stronger infarct tissue may be less affected by the stresses that lead to infarct expansion and remodeling. The change in infarct size from day 1 to day 30 post-MI was twice as large in the $Bgn^{+/0}$ as the $Bgn^{-/0}$, but the difference was not statistically significant. However, because of the variability in infarct size that is common in MI studies, it would be extremely difficult to show a difference without a method of measuring infarct size in the same animals at different time points, such as delayed contrast-enhanced magnetic resonance imaging, even by increasing the number of animals.

Fibrosis of the remote LV is another important component of post-MI ventricular remodeling. Global ventricular collagen deposition is commonly observed with the increase in wall stress resulting from pressure overload and MI. An increase in biglycan expression has been reported in animal models of both pathologies (29, 30). In an aortic banding study, banded rats with carotid pressures of 162 ± 3 mmHg compared to 133 ± 4 mmHg in sham-operated rats showed increased expression of biglycan by fibroblasts (29). Rats in heart failure as a result of MI showed global cardiac induction of biglycan, which the authors hypothesized may have enhanced TGF-β activity and increased collagen deposition (30). They also presented evidence that Angiotensin-II induces biglycan in heart failure, and that this induction can be blocked with an AT1 receptor antagonist, a drug known to slow pathological remodeling. These findings support the trend toward the reduced remote collagen concentration observed in *Bgn*$^{-/0}$ left ventricles. Ventricular wall stress may not have reached the level present in heart failure, which could explain the lack of statistical significance. This potential for attenuated global cardiac collagen deposition may confer a functional advantage to *Bgn*$^{-/0}$ hearts and delay the onset of failure, mimicking the therapeutic actions of AT1 antagonists. In fact, increased liver weight, a manifestation of the systemic congestion that is a hallmark of heart failure, was observed in *Bgn*$^{+/0}$ but not *Bgn*$^{-/0}$ mice 30 days post-MI. Further study will be necessary to discover if heart failure is actually postponed in *Bgn*$^{-/0}$ mice.

In this report, we show for the first time that null expression of the SLRP biglycan is associated with altered collagen ultrastructure and mechanical properties in the mature post-MI scar. This model may also provide a novel avenue for studying the relationship between scar mechanics and the possibility of delayed onset of heart failure.

Acknowledgement: The authors wish to acknowledge Zhuangjie Li, Helen Hwang, Victor Chiu, and Amy Hsieh for their technical assistance. Part of the work reported here was conducted at the National Center for Microscopy and Imaging Research supported by NIH grant P41 RR004050 to Mark H. Ellisman. The remainder was supported by NIH 5P01 HL46345 (Kirk U. Knowlton, Andrew D. McCulloch).

References

1. Borg T.K., Caulfield J.B. (1981) *Fed Proc.* 40: 2037-41.

2. Sussman M.A., McCulloch A., Borg T.K. (2002) *Circ. Res.* 91: 888-898.

3. Pfeffer M.A., Pfeffer J.M., Fishbein M.C., Fletcher P.J., Spadaro J., Kloner R.A., Braunwald E. (1979) *Circ. Res.* 44: 503-512.

4. Holmes J.W., Nuñez J.A., Covell J.W. (1997) *Am. J. Physio. Heart Circ. Physio.* 272: H2123-H2130.

5. Kawaguchi H., Kitabatake A. (1995) *J. Mol. Cell. Cardiol.* 27: 201-209.

6. Schönherr E., Witsch-Prehm P., Harrach B., Robenek H., Rauterberg J., Kresse H. (1995) *J. Biol. Chem.* 270: 2776-2783.

7. Ezura Y., Chakravarti S., Oldberg A., Chervoneva I., Birk D.E. (2000) *J. Cell. Biol.* 151: 779-88.

8. Kuc I.M., Scott P.G. (1997) *Connect. Tissue. Res.* 36: 287-296.

9. Weis S.M., Zimmerman S.D., Shah M., Covell J.W., Omens J., Ross J.J., Dalton N., Jones Y., Reed C.C., Iozzo R.V., et al. (2005) *Matrix Biol.* 24: 313-324.

10. Iozzo R.V., Murdoch A.D. (1996) *FASEB J.* 10: 598-614.

11. Iozzo R.V. (1998) *Annu. Rev. Biochem.* 67: 609-52.

12. Hildebrand A., Romarís M., Rasmussen L.M., Heinegård D., Twardzik DR, Border W.A., Ruoslahti E. (1994) *Biochem. J.* 302: 527-34.

13. Yamamoto K., Kusachi S., Ninomiya Y., Murakami M., Doi M., Takeda K., Shinji T., Higashi T., Koide N., Tsuji T. (1998) *J. Mol. Cell. Cardiol.* 30: 1749-1756.

14. San Martin S., Soto-Suazo M., Ferreira de Oliveira S., Aplin J.D., Abrahamsohn P., Zorn T.M.T. (2003) *Reproduction* 125: 585-595.

15. Lie J.T., Pairolero P.C., Holley K.E., Titus J.L. (1975) *J. Thorac. Cardiovasc. Surg.* 69: 599-605.

16. Ytrehus K., Liu Y., Tsuchida A., Miura T., Liu G.S., Yang X., Herbert D., Cohen M.V., Downey J. (1994) *Am. J. Physiol.* 267: H2383-90.

17. MacKenna D.A., Omens J.H., McCulloch A.D., Covell J.W. (1994) *Am. J. Physiol.* 266: H1007-H1018.

18. Woessner J.F. (1961) *Archives of Biochemistry and Biophysics* 93: 440-447.

19. Harwood F.L., Amiel D. (1992) *J Appl Physiol* 72: 1687-1691.

20. Eyre D.R., Koob T.J., Van Ness K.P. (1984) *Analytical Biochemistry* 137: 380-388.

21. Karlon W.J., McCulloch A.D., Covell J.W., Hunter J.J., Omens J.H. (2000) *Am. J. Physiol. Heart. Circ. Physiol.* 278: H898-906.

22. Goldberg M., Rapoport O., Septier D., Palmier K., Hall R., Embery G., Young M., Ameye L. (2003) *Connect. Tissue. Res.* 44: 184-188.

23. Ameye L., Aria D., Jepsen K., Oldberg A., Xu T., Young M.F. (2002) *FASEB J.* 16: 673-80.

24. Robinson T.F., Cohen-Gould L., Factor S.M. (1983) *Lab. Invest.* 49: 482-498.

25. Vogel K.G., Trotter J.A. (1987) *Coll Relat Res* 7: 105-114.

26. Omens J.H., Miller T.R., Covell J.W. (1997) *Cardiovasc. Res.* 33: 351-358.

27. Bogen D.K., Rabinowitz S.A., Needleman A., McMahon T.A., Abelmann W.H. (1980) *Circ Res* 47: 728-741.

28. Swan H.J.C., Forrester J.S., Diamond G., Chatterjee K., Parmley W.W. (1972) *Circulation* 45: 1097-1110.

29. Ayada Y., Kusachi S., Murakami T., Hirohata S., Takemoto S., Komatsubara I., Hayashi J., Iwabu A., Ninomiya Y., Tsuji T. (2001) *Clin. Exp. Hypertens.* 23: 633-643.

30. Ahmed M.S., Oie E., Vinge L.E., Yndestad A., Andersen G.O., Andersson Y., Attramadal T., Attramadal H. (2003) *Cardiovasc. Res.* 60: 557-568.